Localization and Interaction of *N*-Methyl-D-Aspartate and Non-*N*-Methyl-D-Aspartate Receptors of Lamprey Spinal Neurons

L. E. Moore,*‡ J. T. Buchanan,§ and C. R. Murphey‡

*Equipe de Neurobiologie, C.N.R.S., University of Rennes I, 35042 Rennes, Cedex, France; ‡Department of Physiology and Biophysics, University of Texas Medical Branch, Galveston, Texas 77555 USA; and §Department of Biology, Marquette University, Milwaukee, Wisconsin 53233 USA

ABSTRACT Small volumes of *N*-Methyl-D-Aspartate (NMDA) and non-NMDA excitatory amino acid receptor agonists were applied to localized regions of the dendritic trees of lamprey spinal neurons along their medial-lateral axis to obtain a spatial map of glutamate receptor distribution. Voltage clamp and frequency domain methods were used to obtain quantitative kinetic data of the voltage dependent ionic channels located both on the soma and on highly branched dendritic membranes. Pressure pulses of NMDA applied to the most peripheral regions of the dendritic tree elicited large somatic impedance increases, indicating that the most peripheral dendrites are well supplied with NMDA receptors. Experiments done with kainate did not elicit somatic responses to agonist applications on peripheral dendrites. The data obtained are consistent with the hypothesis that the activation of NMDA receptors by exogenous glutamate is significantly modified by the simultaneous activation of non-NMDA receptors, which shunts the NMDA response. The non-NMDA shunting hypothesis was tested by a combined application of kainate and NMDA to mimic the action of glutamate showing that the shunting effect of non-NMDA receptor activation virtually abolished the marked voltage dependency typical of NMDA receptor activation. These data were interpreted with a compartmental neuronal model having both NMDA and non-NMDA receptors.

INTRODUCTION

The lamprey spinal cord has been used extensively for studies of locomotion and the role of glutamate receptors in synaptic transmission (Grillner et al., 1986, 1987; Rovainen, 1979) including detailed morphological and physiological measurements of synaptic input on dendrites (Christensen, 1983; Christensen and Teubl, 1979). Previous measurements of the effects of neurotransmitters on lamprey spinal neurons have not been localized to specific regions of their dendritic structures (Moore et al., 1987, 1993; Moore and Buchanan, 1993). Excitatory amino acid receptor distribution is of some importance because the normal excitatory transmitter glutamate activates both NMDA and non-NMDA receptors, which may have different distributions on the neuronal tree structure. In the present experiments, the focal application of transmitter was used both to restrict the location of activated receptors and to investigate the interaction of NMDA and non-NMDA excitatory amino acid (EAA) receptor agonists applied simultaneously to spinal neurons. Voltage clamp and impedance methods were used to obtain quantitative kinetic data of the voltage-dependent ionic channels located both on the soma and on highly branched dendritic membranes. Frequency domain methods were used to analyze explicitly the contribution of distally activated NMDA receptors on membrane responses that occur in the soma. The experimentally determined membrane parameters were incorporated into a neuronal model with a dendritic structure (Clements and Redman, 1989).

MATERIALS AND METHODS

Measurements were done on adult silver lampreys (*Ichthyomyzon unicuspis*) from 25 to 35 cm in length. A spinal cord-notochord preparation was used as previously described (Rovainen, 1974; Moore and Buchanan, 1993). The preparation was pinned to the sylgard bottom of the experimental chamber. The chamber was perfused continuously with physiological solution with the direction of fluid flow along the longitudinal axis of the spinal cord. Volumes of about 5–15 nl of excitatory amino acid agonists were ejected from a pressure micropipette, with the tip located within 100 μ of the dorsal surface of the cord, and unless otherwise stated, over the somatic region of an impaled neuron (Fig. 1). The bath perfusion limited the lateral diffusion of agonist after the ejection. The region of the neuron exposed to the agonist was estimated from the observed diameter of ejected volume containing the dye, methylene blue. The diameters ranged from 50 to 150 μ as noted specifically in the text and figure legends. The concentrations in physiological saline of agonists used in the pipettes were 5 mM D-glutamate, 2 mM NMDA, and 0.5 mM kainate. Alternatively, lower concentrations were bath perfused as stated in the figure legends. The physiological saline consisted of (mM): 91 NaCl, 2.1 KCl, 2.6 $CaCl_2$, 1.8 $MgCl_2$, 4 glucose, 20 $NaHCO_3$, bubbled with 95% O_2, 5% CO_2. The intracellular microelectrodes were filled with 4 M potassium acetate having resistances of 50–70 MΩ. The impedance was measured with a sum of sines method (Marmarelis and Marmarelis, 1978) as previously described (Moore et al., 1993; Moore and Buchanan, 1993; Moore and Christensen, 1985).

Neuronal model

A reduced neuronal model was used (Rall 1959, 1969; Redman 1973) that consisted of a soma compartment with the membrane capacitance, C_m, and resistance, R_m, and five identical dendritic compartments each having a capacitance, $t_c \times C_m$, and a resistance, R_m/t_c, where t_c is a fitted scale parameter. The compartments were connected in series by a resistance, R_s, to form an equivalent cylinder cable with an electrotonic length L

Received for publication 23 February 1994 and in final form 25 October 1994.

Address reprint requests to Dr. Lee E. Moore, Department of Physiology and Biophysics, University of Texas Medical Branch, Galveston, TX 77555. Tel.: 409-772-3399; Fax: 409-772-3381; E-mail: lemoore@lamprey.utmb.edu.

0006-3495/95/01/96/08 $2.00

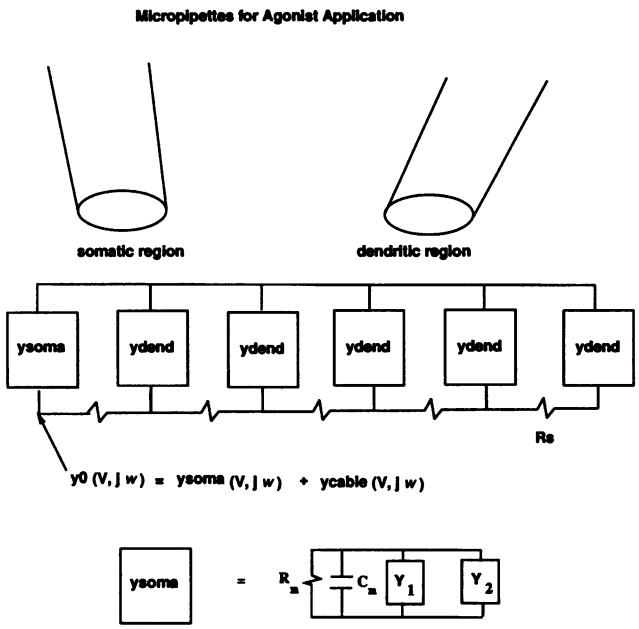

FIGURE 1 Schematic diagram of experimental and analytical setup. Agonists were focally applied by pressure ejection through micropipettes over somatic or dendritic regions of a neuron impaled with a microelectrode in the soma. The frequency domain data were fitted to a neuronal model containing five dendritic compartments with the expression, $y_0[V, j\omega] = y_{soma}[V, j\omega] + y_{cable}[V, j\omega]$, where y_{cable} is the admittance of a multicompartmental cable structure ($y_1[V, j\omega]$), y_{soma} is the admittance of the soma compartment, y_{dend} is the admittance of a single dendritic compartment, and R_s is the series resistance between dendritic compartments. The somatic region includes the soma plus primary dendrites, and the dendritic region refers to the peripheral dendrites. It should be noted that focal application of transmitter over the soma will affect mainly the soma, proximal dendrites, and some peripheral dendrites located dorsal to the cell body.

(see Moore and Christensen, 1985). The data were fitted using a compartmental admittance,

$$y_{soma}(j\omega) = j\omega C_m + \frac{1}{R_m} + G_{ch} + \frac{G_1}{1 + j\omega \tau_1} + \frac{G_2}{1 + j\omega \tau_2}, \quad (1)$$

where G_1 and G_2 are the amplitudes for two voltage dependent conductances having the respective time constants, τ_1 and τ_2 (Hodgkin and Huxley 1952; Mauro et al., 1970; Koch, 1984), and G_{ch} is the sum of the steady-state, voltage-dependent chord conductances. The non-voltage-dependent leakage conductance is $1/R_m$. The passive membrane time constant, $R_m \times C_m$, can only be observed when the voltage-dependent conductances are removed and should not be confused with the relaxation time constants given by the τs. Unless otherwise indicated, the conductances in each of the equivalent cylinder elements were scaled according to the capacitance so that the active conductances were homogenously distributed. In the table and figure legends, the values for the Gs represent the steady-state components of the voltage-dependent conductances (see Moore et al., 1993). The terms of Eq. 1 have been previously derived using the Hodgkin-Huxley formalism (Moore et al., 1993), as follows:

$$G_1 = Gi_1 (V - V_1)(dn_\infty/dV) \quad (2)$$

$$Gi_1 = G_{1max}\, n_\infty, \quad (3)$$

where V is the membrane potential, V_1 is the reversal potential, n_∞ is the steady-state value of a gating variable, Gi_1 is the chord conductance, and G_{1max} is the maximum chord conductance of conductance 1. The slope conductance associated with component 1 is the sum of G_1 and Gi_1. G_1 will have a negative value if $(V - V_1) < 0$. G_2 and Gi_2 for component 2 can be given by expressions analogous to Eqs. 2 and 3. Finally, $G_{ch} = Gi_1 + Gi_2$, which is thus the sum of the steady values of the individual chord conductances.

The driving point admittance in the soma was computed by sequentially adding in parallel the peripheral compartmental admittances, $y_n[V, j\omega]$, including the inter-compartmental resistance, R_s, with the distal admittance as each compartmental admittance is summed. Each equivalent cylinder compartment has an admittance identical to the other dendritic compartments, $y_{dend}[V, j\omega]$, which is a scaled version of y_{soma},

$$y_{dend}[V, j\omega] = t_c \times y_{soma}[V, j\omega]. \quad (4)$$

The equations for five dendritic compartments, with y_4 representing the most peripheral, are as follows:

$$y_4[V, j\omega] = y_{dend}[V, j\omega] + (y_{dend}[V, j\omega]/(R_s \times y_{dend}[V, j\omega] + 1)) \quad (5)$$

$$y_3[V, j\omega] = y_{dend}[V, j\omega] + (y_4[V, j\omega]/(R_s \times y_4[V, j\omega] + 1)) \quad (6)$$

$$y_2[V, j\omega] = y_{dend}[V, j\omega] + (y_3[V, j\omega]/(R_s \times y_3[V, j\omega] + 1)) \quad (7)$$

$$y_1[V, j\omega] = y_{dend}[V, j\omega] + (y_2[V, j\omega]/(R_s \times y_2[V, j\omega] + 1)) \quad (8)$$

$$y_0[V, j\omega] = y_{soma}[V, j\omega] + (y_1[V, j\omega]/(R_s \times y_1[V, j\omega] + 1)), \quad (9)$$

where $y_n[V, j\omega]$ represents the progressively summed admittances for $n + 1$ compartments (Fig. 1). For five dendritic compartments $n = 1$–4, and the final sum, $y_0[V, j\omega]$, is the admittance measured in the soma. Additional dendritic compartments are simply added by extending n. The "passive" electrotonic length, L, was computed as the ratio of the length of the dendritic cable $(n + 1)$ and the space constant, $\lambda = (R_m/R_s)^{1/2}$ in units of compartments; thus, $L = (n + 1)/\lambda$.

The parameters of Eq. 9 were estimated from admittance data taken at individual membrane potentials using a steepest descent algorithm (FindMinimum function, Mathematica, Wolfram Research, Inc., Champaign, Il) to minimize the square of the difference between the model and data. Following the procedures described previously (Moore and Buchanan, 1993), the control data at hyperpolarized values and without NMDA were initially fitted estimating only the passive parameters, C_m, R_m, and R_s. The passive parameters were then fixed when estimating G_1, G_2, τ_1 and τ_2 for NMDA data (Table 1). The term negative conductance, frequently used in the presentation of these results, simply means that G_1 has a negative value. Although Eqs. 2 and 3 give an interpretation of the Gs of Eq. 1, the values for the Hodgkin and Huxley parameters were not estimated. Such an estimation has been done (Murphey et al., 1994) using a more extensive potential range.

RESULTS

Previous studies have shown that both bath applied (Grillner and Wallén, 1985; Wallén and Grillner, 1987) and focally applied NMDA over the soma led to significant activation of EAA receptors, even in the presence of 1.8 mM Mg^{2+} ions (Moore and Buchanan, 1993). There is a partial Mg^{2+} block at the resting potential; however, 100–200 μM NMDA will depolarize lamprey neurons and initiate fictive locomotion. Hyperpolarizations of the order of 20 mV are necessary to obtain a complete Mg^{2+} block of the NMDA receptor in the lamprey Neurons (Moore et al., 1993; Moore and Buchanan, 1993). These two methods of NMDA activation have been directly compared on the same cell in Fig. 2. As reported previously (Moore et al., 1993), the phase of the impedance is extremely sensitive to membrane potential, exhibiting swings from 0 to −180° when the membrane was depolarized by 25 mV in the presence of NMDA. As illustrated in Fig. 2, bath application of 0.1 mM NMDA produced a larger drop in the magnitude of the impedance and a slightly more negative phase than focal application of 2 mM NMDA. This lesser effect of focal application is consistent with the more

TABLE 1 Parameter values

Exp	V_m (mV)	C_m (nF)	R_m (MΩ)	R_s (MΩ)	t_c	t_i	G_{ch} (nS)	G_1 (nS)	τ_1 (ms)	G_2 (nS)	τ_2 (s)	Fig.
Ctl	−72	0.83	105	4.9	0.12							2
Ctl	−97	0.83	105	4.9	0.12							2
F-N	−72	0.83	105	4.9	0.12	0.12	11.7	−35	0.01	8.7	0.76	2
B-N	−72	0.83	105	4.9	0.12	0.12	14.6	−52	0.01	8.7	0.76	2, 3
B-N	−77	0.83	105	4.9	0.12	0.2	4.0	−26	0.01	0		6
+FK	−77	0.83	23	4.9	0.12	0.2	4.0	−26	0.01	0		6
Ctl	−84	0.98	20	0.84	1.1							4
F75	−84	0.98	20	0.84	1.1	1.1	41	−61	0.01	107	5	4
F100	−84	0.98	20	0.84	1.1	1.1	36	−65	0.01	185	5	4
F50	−84	0.98	20	0.84	1.1	1.1	36	−77	0.01	200	5	5

The first column, Exp, defines the experimental conditions as follows: Ctl, control; F-N, focal application of NMDA, B-N bath application of NMDA; FK, focal application of kainate in the presence of B-N; F-75, focal application of NMDA 75 μ from midline of spinal cord; F-100, focal NMDA application 100 μ from midline; F-50, focal NMDA application 50 μ from lateral edge of spinal cord. The subsequent columns are V_m, membrane potential; C_m, soma membrane capacitance; R_m, soma membrane resistance; R_s, intercompartmental resistance; t_c, ratio of dendritic compartmental and soma capacitance; t_i, ratio of dendritic compartmental and soma G_{ch}, G_1, and G_2; Fig., the figure in which the model fits and data are shown.

restricted activation of the neuron's dendritic tree by the small volume of NMDA from the pipette (see below). In both cases, NMDA application led to a decrease in the impedance compared to the control value at −72 mV. This neuron is an example of NMDA activation leading to a decrease in the impedance rather than the previously reported increase (Moore et al., 1993; Moore and Buchanan, 1993). In the absence of applied NMDA, further hyperpolarization to −97 mV did not produce an impedance increase compared with −72 mV, which suggests that no voltage-dependent conductances of this cell were activated in the membrane potential range, −72 to −97 mV.

In contrast to chord conductances, which are always positive, slope conductances are either positive or negative. The measurement of a small signal admittance function can be viewed as the determination of a slope conductance at different frequencies. The algebraic addition of negative and positive slope conductances may lead to a smaller net conductance, i.e., a counterintuitive decrease in a positive conductance when an additional conductance (negative) is activated. The physiological relevance of this phenomenon has been demonstrated by an enhancement of electrotonic synaptic potentials due to a TTX-sensitive impedance increase evoked by a subthreshold depolarization (Buchanan et al., 1992). Thus, activation of a negative slope conductance, such as that induced by NMDA or voltage-dependent calcium or sodium channels, causes an impedance increase if the resulting net conductance is positive. However, if the activated negative conductance is sufficiently large to give a net negative value, then the measured magnitude of the absolute value of the impedance will decrease from its maximum.

The magnitude of the impedance is always a positive value, because it is determined from the absolute value of the sum of the squares of the real and imaginary parts of the complex impedance, either of which can be negative. Thus, if the NMDA-activated conductance has a net negative value that exceeds the control positive conductance, then the impedance will decrease below its resting level as in Fig. 2. This result can only be obtained under voltage clamp conditions because a net negative conductance is highly unstable and generally leads to oscillations (Moore and Buchanan, 1993).

Although the neuron of Fig. 2 shows an impedance decrease with NMDA activation at −72 mV, this neuron also shows an impedance increase for the very limited potential range of −97 to −87 mV (see Fig. 3 and control of Fig. 2). This occurs because activation of the negative NMDA conductance algebraically adds with all other conductances to give a smaller positive value, thus, an impedance increase. Finally, from −87 to −72 mV the impedance magnitude then decreases. An impedance increase (see below) is seen over a wider potential range (Moore and Buchanan, 1993; Moore et al., 1993) with lower levels of NMDA activation and occurs under conditions where the system is stable.

The points raised in the above discussion are illustrated by the recorded voltage clamp currents. Under control conditions the current responses to voltage steps are positive for depolarizing steps and negative for hyperpolarizing potentials (Fig. 2, Control *inset*). However, in the presence of NMDA (Fig. 3, *inset*), the responses are reversed relative to the holding current, i.e., a negative, inward current flows for a depolarizing step and a less negative current is elicited for the hyperpolarizing condition. It is immediately apparent that the steady-state conductance, $\delta I/\delta V$, for both hyper- and depolarizing voltage clamp steps is negative in Fig. 3 (NMDA present) and positive in Fig. 2 (Control *inset*). Furthermore, because the current responses of the opposite, unequal voltage steps of Fig. 3 (*inset*) are about the same, it is evident that the negative slope conductance is greater in the depolarizing direction. Finally, Fig. 2 (NMDA *inset*) illustrates that focal application of NMDA leads to both a smaller net inward current at the holding level of −77 mV and a lesser current response to a depolarizing voltage clamp step.

The potential range over which the system becomes unstable begins at a balance point when the inward and outward currents are equal. In other words, at the balance point or the beginning of instability, the steady-state inward and outward currents that are evoked with a small signal voltage displacement are equal and opposite at some frequencies. This means that the total steady-state membrane conductance (D.C. or low frequency value of admittance) approaches zero and the principle circuit element left in the membrane is capacitative. A pure capacitance would have a linear magnitude function

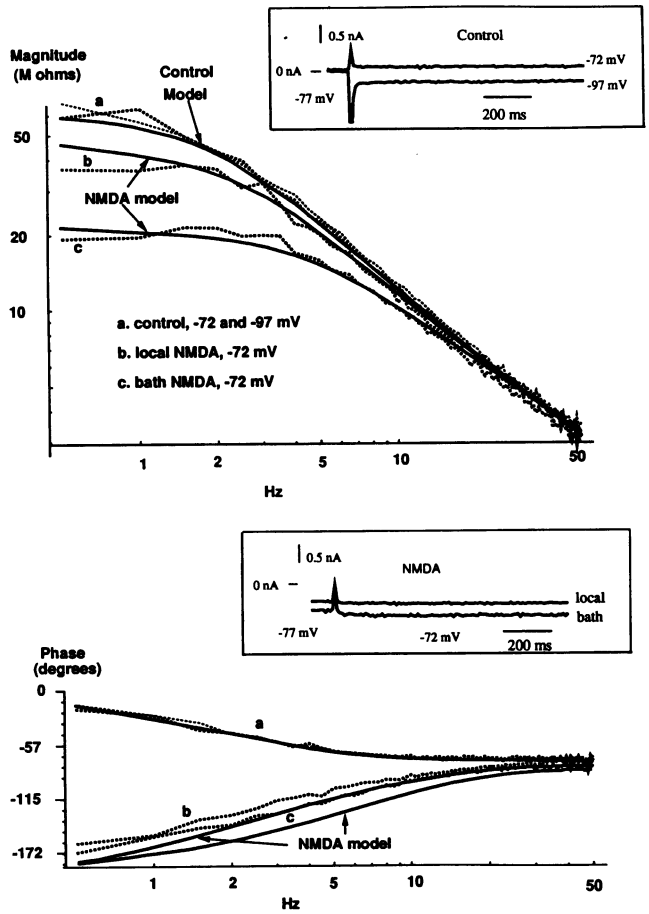

FIGURE 2 Comparison of focal versus bath application of NMDA. Focal application (*b*) had similar, although slightly smaller, effects as bath application. In Figs. 2 and 3, the dashed lines represent the data and the solid lines are the magnitude and phase functions of equation (9) with the parameters given below. Parameters for six compartmental model, where t_c is the scale factor for the capacitance in the dendritic compartments compared to the soma: (*a*) The thin dashed lines represent the data at −72 mV, and the thick dashed lines at −97 mV. Control, −72 and −97 mV: C_m = 0.83nF, R_m = 105 Mohm (9 nS), t_c = 0.12; C_n = 0.10 nF, R_s = 4.9 Mohm, L = 0.38; (b) local NMDA model (upper smooth curve), -72 mV: G_1= −35 nS; τ_1 = 13 μs; G_2 = 8.73 nS, τ_2 = 0.76 s, G_{ch} = 11.7 nS. The parameters for the bath NMDA model (*lower smooth curve*) are given in Fig. 3. The current versus time responses of the same neuron, just before the sum-of-sines signal. In the control insert, a step to −72 mV from the holding level, V_h, −77 mV, gave a net outward current and a step to −97 mV gave a net inward current. The NMDA insert shows that in the presence of bath or locally applied NMDA, a step to −72 mV from −77 mV resulted in a net inward current. While both local and bath-applied NMDA produced inward currents, the bath effect was larger, consistent with the results from the impedance functions. Cell #78B27.

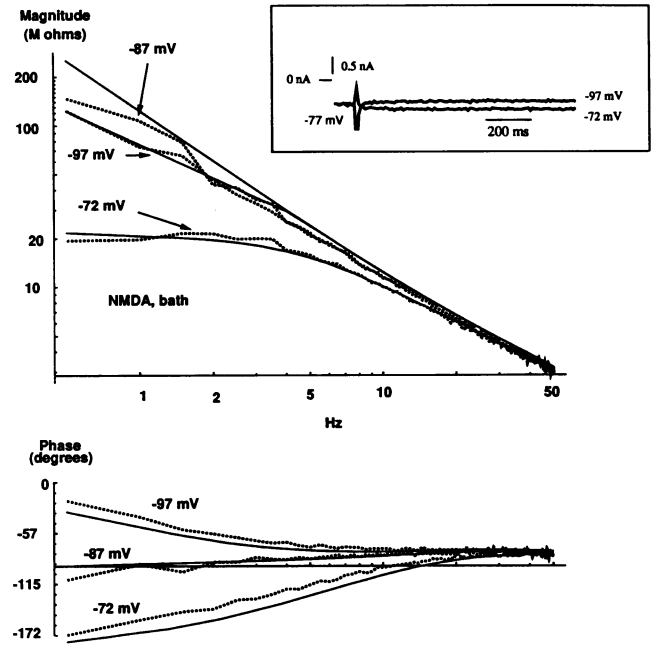

FIGURE 3 Voltage dependence of NMDA effects. NMDA (0.1 mM) was bath-applied, and the cell was recorded in voltage-clamp mode. In this cell NMDA produced a decrease in the magnitude of the impedance function, whereas the phase lag showed its typical increase. In this case, the negative conductance induced by NMDA at −72 mV (−52 nS) was more than two-fold greater than the positive conductance. Parameters for six compartmental model: NMDA bath, −97 mV: C_m = 0.83 nF, R_m = 105 Mohm, t_c = 0.12, C_n = 0.10 nF, R_s = 4.9 Mohm, G_1 = −6.6 nS, τ_1 = 3 μs, G_2 = −0.37 nS, τ_2 = 0.43 s; G_{ch} = 1.4 nS; NMDA bath, −87 mV: G_1 = −13.1 nS, τ_1 = 5.4 μs; G_2 = 0.39 nS; τ_2 = 0.55 s; G_{ch} = 3.3 nS; NMDA bath, −72 mV: G_1 = −52 nS, τ_1 = 13 μs; G_2 = 8.73 nS, τ_2 = 0.76 s, G_{ch} = 14.6 nS; Current versus time responses of the same neuron, just before the sum-of-sines signal. In the NMDA, bath insert, the hyperpolarizing step from −77 to −97 mV gave an outward, rather than the control inward, current relative to the level at the holding potential. This can be explained as a turning off of some of the inward NMDA current. Cell #78B27.

and a phase at all frequencies of 90°. For the NMDA-bathed neuron of Fig. 3, the null point is near −87 mV, where the magnitude function is nearly linear and the phase at all frequencies is near −90 °, as if the system were mainly capacitative. Thus, at the potential of -87 mV, the positive and negative conductances balance each other such that the net conductance approaches zero. This point represents the maximum impedance which decreases at potentials in either direction because the net conductance increases in either a positive or negative direction. In the hyperpolarizing direction where the net conductance is positive, the system is stable; however, in the depolarizing direction, the net conductance is negative and the system is unstable. Under the latter conditions, the system typically shows oscillatory behavior (Moore and Buchanan, 1993).

In Figs. 4 and 5 the focal application was limited to a 50 μ width (see below) to apply NMDA at different locations on the neuron. In contrast to the neuron of Figs. 2 and 3, the effect of a more limited activation of NMDA receptors on the cell of Fig. 4 always showed an enhancement of the impedance, which will occur if the negative conductance is less than twice the positive conductance. In Fig. 3 the more widespread application of NMDA was either uniform or over a large focal region of about 100 μ in diameter centered over the soma. It should be noted that focal application to the somatic region will also activate proximal dendrites and some peripheral dendrites located dorsal to the soma.

Under the conditions of limited NMDA application illustrated in Figs. 4 and 5, the phase function remains less negative than −90° with no tendency to approach −180 °.

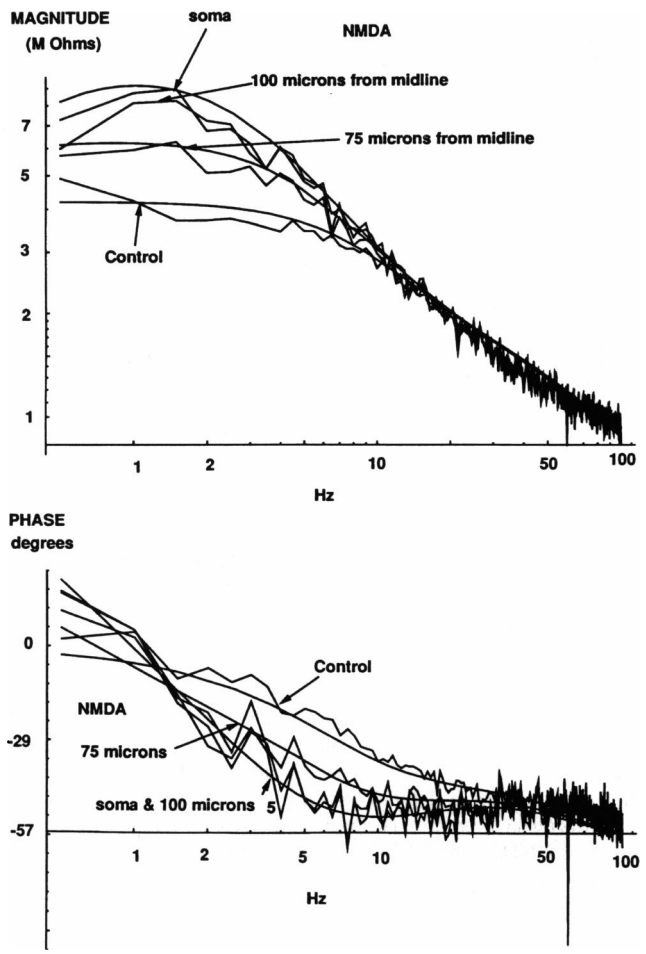

FIGURE 4 Medial application of NMDA. NMDA was applied from a pipette onto a cell in the presence of 1 μM TTX recorded in current clamp using small pressure pulses of NMDA with the pipette located various distances from the midline. No effects were observed within 50 μ from the midline (not shown). The first effect was observed when the pipette was moved 25 μ further to 75 μ, and the response became maximal at 100 μ. The smooth lines are model fits superimposed on connected data points. Model parameters for a six compartmental model were as follows: Control and 50 μ lateral to midline: C_m = 0.98 nF, R_m = 20 Mohm, t_c = 1.1, R_s = 0.84 Mohm, L = 1.1; 75 μ: R_m = 20 Mohm, G_1 = −61 nS, τ_1 = 0.01 ms, G_2 = 107 nS, τ_2 = 5 s, G_{ch} = 41 nS; 100 μ: G_1 = −65 nS, τ_1 = 0.01 ms, G_2 = 185 nS, τ_2 = 5s, G_{ch} = 36 nS, V_r = −84 mV.

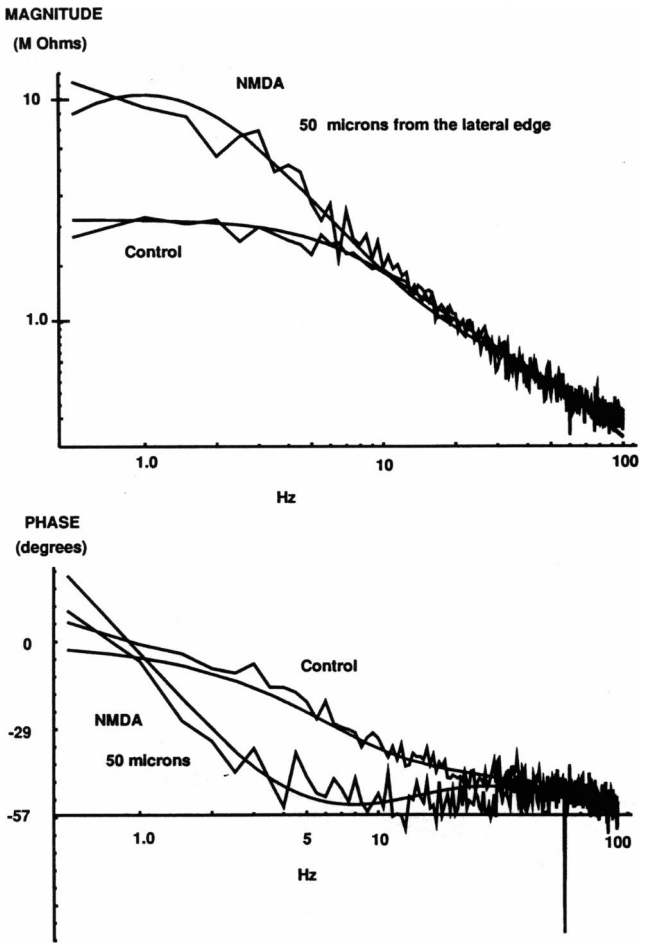

FIGURE 5 Peripheral application of NMDA. Application of NMDA to the peripheral dendrites, 50 μ from the lateral edge of the spinal cord, gave a maximal response. Thus, NMDA receptors exist on the peripheral dendrites. The same pipette and pressure pulse size were used for all illustrated impedance functions in Figs. 4 and 5. The smooth lines are model fits superimposed on connected data points. The NMDA model had no voltage-dependent parameters in the soma, i.e., G_1 = 0, G_2 = 0, and G_{ch} = 0. The values given are for each of the five dendritic compartments. The control values are given in the Fig. 4 legend; NMDA: G_1 = −85 nS, τ_1 = 0.01 ms, G_2 = 220 nS, τ_2 = 5 s, G_{ch} = 40 nS, V_r = −84 mV. Cell # 21G23.

A phase function that exceeds −90 ° is indicative of a net negative conductance. If the activated negative conductance does not exceed the positive conductance the phase function will not exceed −90°, as is the case for all net positive conductance systems. The activation of the negative conductance in this cell is thus below the balance or null point so that the overall net effect is an impedance increase. In part this may simply be due to an activation of fewer receptors.

One additional hypothesis to explain the lack of a net negative conductance in the cell of Fig. 4 is that the number of activated NMDA receptors could be lower in the somatic region compared with peripheral dendrites such that it would be difficult to obtain a net negative conductance from an electrode in the soma. To test this hypothesis and to determine whether the peripheral dendrites of lamprey spinal neurons can respond to NMDA, the pressure pipette was used to map the medial-lateral axis of the dendritic tree. In the lamprey, dendrites radiate from each soma and extend to near the midline and to the lateral edges of the spinal cord. By applying small volumes of agonist, it is possible to expose restricted focalized regions of the dendritic tree and thus map the sensitivity of the neuron by moving the pipette along the cell's medial-lateral axis.

The degree of localization of agonist application was evaluated by progressively moving the NMDA pipette from the midline toward the lateral edge of the cord (a distance of 550 μ for the experiment of Fig. 4) in 25 μ increments giving pressure pulses at each location and measuring the impedance function. The largest response in Fig. 4 was seen with the pipette over the soma, which was about 200 μ from the

midline. At the midline and up to 50 μ lateral to the midline, there was no response to NMDA. At 75 μ, however, a large increase in the magnitude of the impedance, characteristic of NMDA receptor activation, was observed. Therefore, the effective radius of the ejected NMDA solution appeared to be less than 25 μ. This response increased to the maximally observed level when the NMDA was applied 100 μ from the midline.

The responsiveness of the lateral dendrites was then tested by positioning the pipette 50 μ from the lateral edge of the spinal cord, which was about 350 μ from the cell body. The same-sized pressure pulse of NMDA used above elicited an increase in the impedance even greater than that observed by direct application over the somatic region and proximal dendrites (Fig. 5). Because the response observed at the soma was approximately one "passive" electrotonic length away, the quantity of NMDA receptors is likely to be greater in the periphery than the central region. Such behavior could occur if the density of NMDA receptor sites was homogeneous throughout the neuron; however, more receptors would be present in the periphery because of the larger dendritic area.

The term "passive" electrotonic length, L, is used to emphasize the difference between the electrotonic length under resting or passive conditions compared with what would occur during steady-state channel activation. If positive dendritic conductances are increased, it is clear that the electrotonic length increases and peripheral events measured with a somatic electrode will be attenuated (Redman, 1973). However, if negative slope conductances are activated, the impedance of dendritic regions may increase and lead to a decreased electrotonic length that has been shown to enhance synaptic potentials (Buchanan et al., 1992). Thus, peripheral NMDA receptors have the built-in property of increasing the membrane impedance and making their presence felt at the soma far more effectively than classical shunting receptors. Under these conditions, there is no particular advantage to have NMDA receptors centrally because their effect will be easily propagated from peripheral regions. Similar experiments with peripheral application of kainate had no effect on the impedance measured at the soma.

In contrast to the effects of NMDA, somatic application of glutamate led to minimal and variable effects on the impedance properties of spinal neurons (Moore and Buchanan, 1993). These results are in part consistent with the dual activation by glutamate of both NMDA and non-NMDA receptors with a response that would be the summation of positive and negative effects. In addition, no indication of any voltage-dependent glutamate effect was observed in these experiments. This is a highly significant negative result because it indicates that whatever the activation of NMDA receptors that occurs with glutamate, its observation in the soma is attenuated by the simultaneous activation of non-NMDA receptors. One way this could occur is through a shunting effect by more centrally distributed non-NMDA sites of the peripheral NMDA receptors.

The non-NMDA shunting hypothesis was tested by the experiment of Fig. 6 where a combined application of kainate

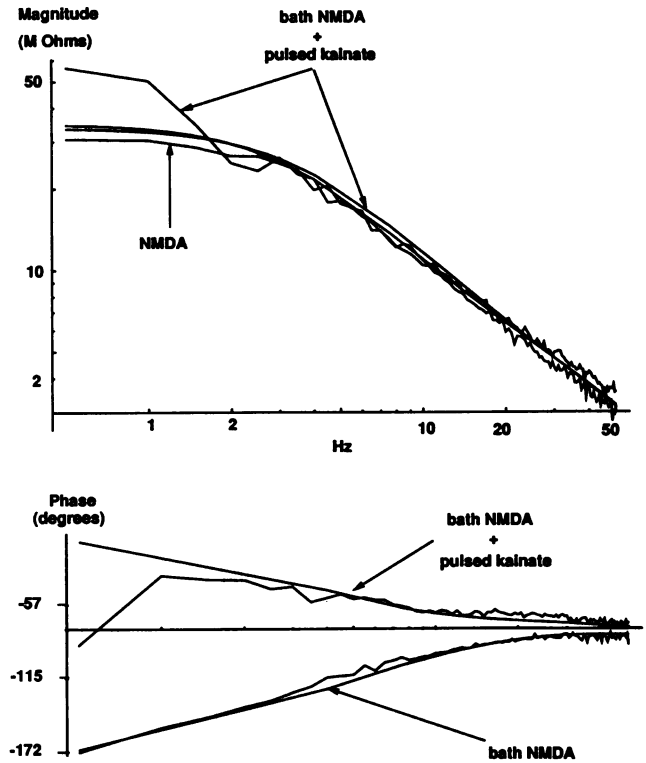

FIGURE 6 The effect of kainate on NMDA responses. NMDA (0.1 mM) was bath-applied and showed a large phase lag (near $-180°$ at low frequencies) in voltage clamp mode. When kainate (0.5 mM) was applied to the cell from a pipette in the presence of NMDA, the phase lag decreased dramatically. Voltage-clamp recording in the presence of 1 μM TTX. The smooth lines are model fits superimposed on connected data points. Model parameters for a soma with five dendritic compartments where t_i is the scale factor for relaxation amplitudes of the ionic conductances ($t_i \times G_1$ and $t_i \times G_{ch}$) in the dendritic compartments compared to the somatic compartment: Passive parameters: C_m = 0.83 nF, R_m = 105 MΩ, t_c = 0.12, R_s = 4.9 Mohm; NMDA: t_i = 0.20, G_1 = -26 nS; τ_1 = 0.01 ms; G_2 = 0 nS; G_{ch} = 4 nS; NMDA + Kainate: R_m = 23 MΩ (43 nS), V_h = -77 mV. Cell #78B27.

and NMDA was done to mimic the action of the endogenous excitatory amino acid transmitter glutamate. The cell was first bathed in 0.1 mM NMDA, and its impedance function was measured, and the cell exhibited a phase function that approached $-180°$ at low frequencies. Upon focal application of kainate (0.5 mM) over the soma, the most prominent effect was the reduction of the NMDA-induced phase lag, with minimal effects on the magnitude. In the NMDA case, the curve-fitted model drawn through the experimental points consisted of a single negative conductance reflecting that the predominant effect was an activation of inward current. The model used for the data obtained after kainate application has the same parameters plus a shunted membrane resistance (see legend of Fig. 6 and Table 1). The lack of an effect on the magnitude function, despite an increased shunt conductance, is an example of a change in the sign of the net conductance from negative to positive with no significant effect on its absolute value as observed by the magnitude function. Thus, these results show that the simultaneous activation of NMDA and kainate receptors can lead to a

complex addition of conductance changes that must be analyzed with a membrane model rather than as simple potential responses. This experiment of applying kainate or quisqualate focally to a spinal cord bathed in NMDA was done on five neurons with similar reductions of the NMDA effect.

DISCUSSION

The distribution of NMDA and non-NMDA receptors critically determine the nature of synaptic responses. The colocalization of NMDA and non-NMDA receptors (Bekkers and Stevens, 1989; Jones and Baughman, 1991) provides a clear basis for complex interactions that will depend on the relative densities of the two receptor types and their kinetic properties. The physiological determination of spatial profiles of receptors on dendritic trees is likely to be confounded by membrane properties. The use of iontophoretic electrodes for focal application has been used in cultured neurons to demonstrate "hot spots" of glutamate receptors showing less spatial resolution for NMDA compared with non-NMDA receptors (Jones and Baughman, 1991). One basis for this difference could be the desensitization of the non-NMDA response. Alternatively, the findings presented in this paper show that NMDA induces a profound negative conductance that could lead to an increase in the space constant. A change in the electrotonic length of a dendrite would alter the spatial resolution measured by focally applying NMDA near a receptor site.

The issues concerning the effect of spatial resolution also apply to the mechanisms that generate the time course of synaptic currents. A number of groups have demonstrated that glutamatergic synapses are generally composed of NMDA and non-NMDA responses (Forsythe and Westbrook, 1988; Lester et al., 1990) where the former are characterized by slow channel kinetics (Hestrin et al., 1990a, b). Furthermore, different cell types appear to have variable NMDA kinetic properties (Perouansky and Yaari, 1993). The ability to determine the actual mechanism of the synaptic current time course rests on a detailed knowledge of the receptor distribution and accurate determination of channel kinetics is needed before any definitive conclusions can be drawn concerning the relative role of structure versus membrane properties.

The filter properties of an excitable membrane that are the consequence of the voltage-dependent conductances can be expressed in quantitative terms to show how the usual kinetic processes give rise to specific filter characteristics (Moore and Tsai, 1983; Moore et al., 1988; Moore and Christensen, 1985; Yoshii et al., 1988). Such considerations are especially revealing when clarifying a negative conductance (Fishman et al., 1979, 1983). The sign of G_1 in Eq. 2 is determined by both the driving force for ion movement, $(V - V_e)$, and dn_∞/dV. For outward currents, where activation occurs and when V is more depolarized than V_e, G_1 is positive. However, for inward currents, for example those due to sodium or calcium ions, $V - V_e$ is of the opposite sign and G_1 is negative, hence, a negative slope conductance. As a consequence, the admittance for a single ionic species (Mauro et al. 1970) becomes

$$Y = G_o - \frac{|G_1|}{1 + \omega^2 \tau_1^2} + j\omega\left[\frac{C_m + |G_1| \times \tau_1}{1 + \omega^2 \tau_1^2}\right] \quad (10)$$

where G_o is the total frequency independent conductance ($G_o = G_{ch} + 1/R_m$), $G_1 < 0$, and $|G_1|$ is the absolute value of G_1. It is clear from Eq. 2 that the capacitative part, given by $j\omega$ times a factor, is composed of two additive terms, the normal capacitance and a second positive term due to the negative conductance. Thus, the filter characteristics of a negative conductance can partially be expressed as an additional capacitance at low frequencies. Similarly, the filter characteristics of a positive conductance can be viewed as a decreased capacitance at low frequencies. At D.C. the value of Y becomes the difference between G_o and $|G_1|$, which can have a net negative value, i.e., the net slope conductance, $\delta I/\delta V$, would be negative. The magnitude function of Eq. 10 is

$$Y^2 = \left(G_o - \frac{|G_1|}{1 + \omega^2 \tau_1^2}\right)^2 + \omega^2\left(C_m + \frac{\tau_1 |G_1|}{1 + \omega^2 \tau_1^2}\right)^2. \quad (11)$$

Equation 11 is identical in form to that of a positive conductance, except that as a consequence of the negative value of G_1, the signs preceding the absolute value of G_1 are opposite. As discussed above, this leads to an increased apparent capacitance and a conductance term,

$$(G_o - |G_1|/(1 + \omega^2 \tau_1^2))^2,$$

that may increase rather than fall with frequency. The consequence of this difference is that the magnitude function for a single negative conductance does not generally show a minimum, hence the impedance of the system does not usually resonate. An exception to this rule can occur if $|G_1| > G_o$, then an impedance resonance is possible.

The data of Figs. 4 and 5 clearly demonstrate that NMDA receptors are present on both peripheral and proximal dendritic trees of spinal neurons. The increased apparent capacitance induced by NMDA activation is shown in Fig. 6 in the data and the model by the lower level of the phase function at high frequencies when NMDA was not shunted by kainate. The ability to observe this effect requires a proximal distribution of NMDA receptors, otherwise, the cable properties of the dendritic tree would filter the high frequency effects such that they could not be observed with an electrode in the soma. In some neurons, such as those shown in Figs. 4 and 5, the high frequency effects are not observed. This could occur for two reasons: 1) there was no net negative conductance during NMDA activation, or 2) the net negative conductance was present only in the periphery. The presence of high frequency shifts related to NMDA activated negative conductances have been observed in four neurons that were investigated during maximal activation of NMDA receptors obtained during bath application of NMDA.

The findings of this paper suggest that voltage-dependent conductances in neuronal structures have at least two

important roles, (1) the propagation of nonlinear signals, and (2) dynamic control of the linear cable properties that are, in fact, voltage-dependent. The linear, steady-state properties are clearly relevant in synaptic processing, because many synaptic events fulfill the small signal requirement needed for linear analysis. Thus, the subthreshold responses of dendritic membranes with their synaptic sites are determined by the complex interplay of not only the intrinsic membrane conductances, but also those induced by neurotransmitters. In the case of glutamate receptors, the voltage-dependent NMDA receptors are essentially turned on by non-NMDA receptors because of their initial depolarization; however, excess activation of non-NMDA receptors can shunt the NMDA response. Combined with inhibitory synapses, these mechanisms provide subtle control of synaptic processing that is likely to play a role in a number of systems.

This work was supported in part by DHHS-R01-MH45796 (U.S.) and C.N. R.S. (France).

REFERENCES

Bekkers, J. M., and C. F. Stevens. 1989. NMDA and non-NMDA receptors are co-localized at individual excitatory synapses in cultured rat hippocampus. *Nature.* 341:230–233.

Buchanan, J., L. E. Moore, P. Wallén, R. Hill, and S. Grillner. 1992. Synaptic transfer function of Mueller axon to spinal neuron in lamprey. *Biol. Cybern.* 67:123–131.

Christensen, B. N. 1983. Distribution of electrotonic synapses on identified lamprey neurons: a comparison of a model prediction with an electron microscopic analysis. *J. Neurophysiol.* 49:705–716.

Christensen, B. N., and W. P. Teubl. 1979. Localization of synaptic input on dendrites of a lamprey spinal cord neurone from physiological measurements of membrane properties. *J. Physiol.* 297:319–333.

Clements, J. D., and S. J. Redman. 1989. Cable properties of cat spinal motoneurones measured by combining voltage clamp, current clamp, and intracellular staining. *J. Physiol.* 409:63–87.

Fishman, H. M., H. R. Leuchtag, and L. E. Moore. 1983. Fluctuation and linear analysis of Na^+ current kinetics in squid axon. *Biophys. J.* 43: 293–308.

Fishman, H. M., D. Poussart, and L. E. Moore. 1979. Complex admittance of Na+ conduction in squid axon. *J. Membr. Biol.* 50:43–63.

Forsythe, I. D., and G. Westbrook. 1988. Slow excitatory postsynaptic currents mediated by N-Methyl-D-Aspartate receptors on cultured mouse central neurones. *J. Physiol.* 396:515–533.

Grillner, S., and P. Wallén. 1985. The ionic mechanisms underlying NMDA receptor induced, TTX resistant, membrane potential oscillations in lamprey neurones active during locomotion. *Neurosci. Lett.* 60:289–294.

Grillner, S., L. Brodin, J. T. Buchanan, P. Wallén, N. Dale, R. Hill, and L. E. Moore. 1986. Excitatory amino acid neurotransmission in the lamprey spinal cord: a key role in the generation of locomotion. *In* Excitatory Amino Acid Transmitters. P. Hicks, D. Lodge, and H. McLennan, editors. Alan Liss, Inc., New York. 293–300.

Grillner, S., P. Wallén, N. Dale, L. Brodin, J. Buchanan, and R. Hill. 1987. Transmitters, membrane properties, and network circuitry in the control of locomotion in lamprey. *Trends Neurosci.* 10:34–41.

Hestrin, S., R. A. Nicoll, D. J. Perkel, and P. Sah. 1990a. Analysis of excitatory synaptic action in pyramidal cells using whole-cell recording from rat hippocampal slices. *J. Physiol.* 422:203–225.

Hestrin, S., P. Sah, and R. A. Nicoll. 1990b. Mechanisms generating the time course of dual component excitatory synaptic currents recorded in hippocampal slices. *Neuron.* 5:247–253.

Hodgkin, A. L., and A. Huxley. 1952. A quantitative description of membrane current, and its application to conduction, and excitation in nerve. *J. Physiol.* 117:500–544.

Jones, K. A., and R. W. Baughman. 1991. Both NMDA and non-NMDA subtypes of glutamate receptors are concentrated at synapses on cerebral cortical neurons in culture. *Neuron.* 7:593–603.

Koch, C. 1984. Cable theory in neurons with active, linearized membranes. *Biol. Cybern.* 50:15–33.

Lester, R. A. J., J. D. Clements, G. L. Westbrook, and G. Jahr. 1990. Channel kinetics determine the time course of NMDA receptor-mediated synaptic currents. *Nature.* 346:565–567.

Marmarelis, P. Z., and V. Z. Marmarelis. 1978. Analysis of Physiological Systems: The White Noise Approach. Plenum Press, New York.

Mauro, A., F. Conti, F. Dodge, and R. Schor. 1970. Subthreshold behavior and phenomenological impedance of the squid giant axon. *J. Gen. Physiol.* 55:497–523.

Moore, L. E., and J. Buchanan. 1993. The effects of neurotransmitters on the integrative properties of spinal neurons of the lamprey. *J. Exp. Biol.* 175:89–113.

Moore, L. E., and B. N. Christensen. 1985. White noise analysis of cable properties of neuroblastoma cells, and lamprey central neurons. *J. Neurophysiol.* 53:636–651.

Moore, L. E., R. H. Hill, and S. Grillner. 1987. Voltage clamp analysis of lamprey neurons: role of N-methyl-D-aspartate receptors in fictive locomotion. *Brain Res.* 419:397–402.

Moore, L. E., R. H. Hill, and S. Grillner. 1993. Voltage clamp frequency domain analysis of NMDA activated neurons. *J. Exp. Biol.* 175:59–87.

Moore, L. E., and T. D. Tsai. 1983. Ion conductances of the surface, and transverse tubular membranes of skeletal muscle. *J. Membr. Biol.* 73:217–226.

Moore, L. E., K. Yoshii, and B. Christensen. 1988. Transfer impedances between different regions of branched excitable cells. *J. Neurophysiol.* 59:689–705.

Murphey, C. R., L. E. Moore, and J. T. Buchanan. 1995. Quantitative analysis of electrotonic structure and membrane properties of NMDA activated lamprey spinal neurons. *Neural Computat.* In press.

Perouansky, M., and Y. Yaari. 1993. Kinetic properties of NMDA receptor-mediated synaptic currents in rat hippocampal pyramidal cells versus interneurons. *J. Physiol.* 465:223–244.

Rall, W. 1959. Branching dendritic trees and motoneuron membrane resistivity. *Exp. Neurol.* 1:491–527.

Rall, W. 1969. Time constants, and electrotonic length of membrane cylinders, and neurons. *Biophys. J.* 9:1483–1508.

Redman, S. J. 1973. The attenuation of passively propagating dendritic potentials in a motoneurone cable model. *J. Physiol.* 234:637–664.

Rovainen, C. M. 1974. Synaptic interactions of identified nerve cells in the spinal cord of the sea lamprey. *J. Comp. Neurol.* 154:189–206.

Rovainen, C. M. 1979. Neurobiolgy of lampreys. *Physiol. Rev.* 59:1007–1077.

Wallén, P., and S. Grillner. 1987. N-methyl-D-aspartate receptor-induced, inherent oscillatory activity in neurons active during fictive locomotion in the lamprey. *J. Neurosci.* 7:2745–2755.

Yoshii, K., L. E. Moore, and B. N. Christensen. 1988. The effect of subthreshold voltage dependent conductances on the transfer function of branched excitable cells. *J. Neurophysiol.* 59:706–716.